Microscopic three-dimensional imaging by digital interference holography

Aaron Dakoff
James Gass
Myung K. Kim
University of South Florida
Department of Physics
Tampa, Florida 33620
E-mail: mkkim@cas.usf.edu

Abstract. *Digital interference holography (DIH) is being developed as a novel method of microscopic 3-D imaging. A number of holographic fields are numerically calculated from optically recorded holograms using a range of wavelengths. Numerical superposition of these fields results in a tomographic representation of the object with narrow axial resolution. We demonstrate the practicality of DIH in microscopic imaging with a set of preliminary experiments, yielding approximately 3 μm of lateral resolution and 10 μm of axial resolution, using a simple optical setup and straightforward numerical algorithms.* © 2003 SPIE and IS&T. [DOI: 10.1117/1.1604784]

1 Introduction

We are developing digital interference holography (DIH) as a novel method of microscopic 3-D imaging by numerical superposition of a number of holographic fields taken with varying wavelengths.[1,2] Unlike some of the other well-developed 3-D microscopic methods such as confocal microscopy and optical coherence tomography, digital interference holography does not involve pixel-by-pixel mechanical scanning of 3-D volume, yet achieves comparable resolutions. In DIH, the holographic interference pattern of an object is generated optically and recorded digitally using a CCD camera. The holographic image field is numerically calculated and the process repeated for a large number of varying wavelengths at regular intervals. Numerical superposition, or digital interference, of the holographic image fields yields the desired 3-D representation of the object. We have demonstrated the practicality of the DIH in microscopic 3-D imaging with a set of preliminary experiments yielding approximately 3 μm of lateral resolution and 10 μm of axial resolution.

A basic strategy in many tomographic imaging techniques is to detect the angular position or propagation distance (time of flight) of reflection or transmission signals using detector arrays or a single scanning detector. The set of angular and distance data for varying source positions is then used to calculate the 3-D coordinates of the object points. This is the case with x-ray computed tomography, magnetic resonance imaging, positron emission tomography, and ultrasound imaging, as well as some optical tomographic methods in diffuse media.[3] The optical tomography is most useful in microscopic imaging because of the short wavelength and the limited penetration depth of most biological surfaces. For example, laser confocal microscopy utilizes aperturing of both the illuminated sample volume and the detector, thereby rejecting all scattered light other than that from the focal volume.[4] More recent developments in optical coherence tomography are basically time-of-flight measurement techniques, utilizing ultra-short laser pulses or continuous wave lasers of very short coherence time.[5–7] In both of these methods the signal is detected one pixel at a time and the 3-D image is reconstructed by scanning the three dimensions pixel by pixel. Although microscanning using piezo actuators is a remarkable art, being able to obtain images frame by frame will have obvious technical advantages.[8]

By recording the phase as well as intensity of light-waves, holography allows reconstruction of the images of 3-D objects, and gives rise to a host of metrological and optical processing techniques.[9] With the advance of computer and electronic imaging technology, it is now very practical and often advantageous to replace portions of holographic procedures with electronic processes. With digital holography, real-time processing of the image is possible, and phase information of the reconstructed field is readily available in numerical form.[10–12] On the other hand, although the hologram produces a 3-D image of the optical field, this does not by itself yield topographic distance information, other than by focusing and defocusing the image points. Distance information can be obtained in time-of-flight type of measurements,[13] or it can also be determined by counting the number of wavelengths or some multiples of it, which is the basis of various interference techniques.[14,15] A well-known technique is the interference of two holograms recorded at two different wavelengths, resulting in a contour interferogram with the axial distance between the contour planes inversely proportional to the difference in wavelengths. In digital holography, it is possible to extend the process to recording and reconstruction
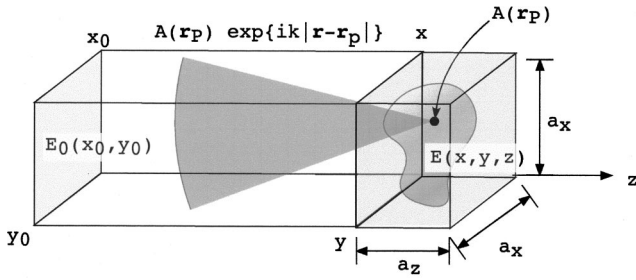
Fig. 1 Configuration of the holographic system. $E_0(x_0,y_0)$ represents the field at the hologram and $E(x,y,z)$ is the field of the 3-D image space near the object position.

of many holograms without introducing any wavelength mismatch. If a number of regularly spaced wavelengths is used for recording and reconstruction, then the peaks of the cosine-squared intensity variation of the two-wavelength interference become sharper and narrower, as when a number of cosines with regularly spaced frequencies are added. This process in effect synthesizes the short coherence length and allows generation of sharp interference peaks as in optical coherence tomography.[16]

2 Basic Principles

To outline the principle of digital interference holography, consider the optical system depicted in Fig. 1. The object is illuminated, either in transmission or reflection, by a laser beam of wavelength λ. A point P on the object scatters the illumination beam into a Huygens wavelet, $A(P)\exp(ik|\mathbf{r}-\mathbf{r}_P|)$, where $A(P)$ is proportional to the amplitude and phase of the scattered wavelet. The $|\mathbf{r}-\mathbf{r}_P|^{-1}$ decrease of the spherical wave amplitude is ignored, and instead we focus our attention on the phase factor of the imaginary exponential. For an extended object, the field at $\mathbf{r}$ is

$$E(\mathbf{r})=\int A(\mathbf{r}_P)\exp(ik|\mathbf{r}-\mathbf{r}_P|)\mathrm{d}^3\mathbf{r}_P,\qquad(1)$$

where the integral is over the object volume. In holography, the amplitude and phase of this field at the hologram plane $z=0$ is recorded, and one of the reconstructed fields is a replica of the object field as described by Eq. (1). We are all familiar with the 3-D perception of holographic images through the parallax effect. However, it does not provide any information on the absolute location and distance of the object, just as one's monocular view of a scene does not provide such information in the absence of other subjective depth cues. Such axial distance information can be obtained by a number of interferometric techniques. For example, if the holographic process is repeated again using a different wavelength $\lambda'=2\pi/k'$ ($|\lambda-\lambda'|=\Delta\lambda$), all other parameters remain the same, and if the two reconstructed fields are added together, then the result is

$$E(\mathbf{r})=\int A(\mathbf{r}_P)\{\exp(ik|\mathbf{r}-\mathbf{r}_P|)+\exp(ik'|\mathbf{r}-\mathbf{r}_P|)\}\mathrm{d}^3\mathbf{r}_P.\qquad(2)$$

Interference of the two wavelengths results in contours of optical path lengths with a period, or beat wavelength, of

$\Lambda=\lambda^2/\Delta\lambda$. This is the basis of the double-exposure contour generation technique in conventional holography. The intensity varies as cosine-squared between the maxima, and the axial resolution is basically the beat wavelength Λ. With digital holography, the process can be extended to any number of holograms. If N holograms are made using wavelengths $\lambda_m=\lambda_0+m\Delta\lambda$ ($m=0,1,2,...,N-1$), and the reconstructed fields are all superposed together, then the resultant field is

$$E(\mathbf{r})=\sum_m \int A(\mathbf{r}_P)\exp(ik_m|\mathbf{r}-\mathbf{r}_P|)\mathrm{d}^3\mathbf{r}_P$$

$$\sim\int A(\mathbf{r}_P)\delta(\mathbf{r}-\mathbf{r}_P)\mathrm{d}^3\mathbf{r}_P\sim A(\mathbf{r}).\qquad(3)$$

That is, for a large enough number of wavelengths, the resultant field is proportional to the field at the object and is nonzero only at the object points. This can also be viewed as a Fourier transform process between the axial distance and the wavelengths.[17,18]

In Eq. (3), the sum of imaginary exponentials is a delta function only if the wavenumber k_m ranges over all real numbers. In practice, if one uses a finite number N of wavelengths at regular intervals of $\Delta\lambda$, then the object image $A(\mathbf{r}_P)$ repeats itself (other than the diffraction/defocusing effect of propagation) at the beat wavelength $\Lambda=\lambda^2/\Delta\lambda$, with axial resolution $\delta=\Lambda/N$. By use of appropriate values of $\Delta\lambda$ and N, the beat wavelength Λ can be matched to the axial extent of the object, and δ to the desired level of axial resolution. Note that for a given level of axial resolution, the required range of wavelengths $N\Delta\lambda$ is the same as the spectral width of low-coherence or short-pulse lasers in optical coherence tomography.

3 Numerical Procedure

The numerical procedure for digital interference holography proceeds as follows. First, at a given laser wavelength λ_0, the holographic interference pattern ($|H|^2$) of the object (O) and reference (R) is generated optically and recorded digitally by a CCD camera. Zero-order diffraction is eliminated by subtracting out the object ($|O|^2$) and the reference ($|R|^2$) from the hologram, leaving

$$|H|^2-|O|^2-|R|^2=OR^*+O^*R.\qquad(4)$$

This is taken as the field $E_0(x_0,y_0)$ at the hologram ($z=0$), defined on a square of physical size $a_x\times a_x$ with $n_x\times n_x$ pixels. Starting from $E_0(x_0,y_0)$, the holographic image field $E(x,y,z)$ near the object's image position is then calculated in a volume of physical size $a_x\times a_x\times a_z$ with $n_x\times n_x\times n_z$ pixels. Usually, $a_z=\Lambda$ and $n_z=N$.

The diffraction field $E(x,y;z)$ that starts as $E_0(x_0,y_0;0)$ and propagates along the z direction is calculated as the integral of the Huygens wavelets[19]:

$$E(x,y)=\int \mathrm{d}x_0\mathrm{d}y_0 E_0(x_0,y_0)$$

$$\times\exp\{ik[(x-x_0)^2+(y-y_0)^2+z^2]^{1/2}\}$$

$$=E_0(x,y)\oplus S_H(x,y),\qquad(5)$$

where the symbol $\oplus$ represents convolution and the Huygens point transfer function (PTF) is given by

$$S_H(x,y) = \exp[ik(x^2+y^2+z^2)^{1/2}]. \tag{6}$$

The convolution is calculated using three Fourier transforms

$$E(x,y) = 2\pi \cdot F^{-1}\{F[E_0(x,y)]F[S_H(x,y)]\}. \tag{7}$$

The calculation simplifies significantly if one uses the Fresnel approximation of the PTF:

$$E(x,y) \approx \int dx_0 dy_0 E_0(x_0,y_0)$$
$$\times \exp\left\{ikz + ik\frac{(x-x_0)^2}{2z} + ik\frac{(y-y_0)^2}{2z}\right\}$$
$$= E_0(x,y) \oplus S_F(x,y), \tag{8}$$

and

$$S_F(x,y) = \exp\left[ikz + \frac{ik}{2z}(x^2+y^2)\right]. \tag{9}$$

In fact, Eq. (8) is a single Fourier transform:

$$E(x,y) \approx \exp\left[\frac{ik}{2z}(x^2+y^2)\right] \int dx_0 dy_0 E_0(x_0,y_0)$$
$$\times \exp\left\{ikz + \frac{ik}{2z}(x_0^2+y_0^2) - \frac{ik}{z}(xx_0+yy_0)\right\}$$
$$= \exp\left[\frac{ik}{2z}(x^2+y^2)\right]$$
$$\times F\{E_0(x_0,y_0)S_F(x_0,y_0)\}[\kappa_x,\kappa_y], \tag{10}$$

with respect to the spatial frequencies $\kappa_x = kx/z$, $\kappa_y = ky/z$. We have made use of both the Huygens and Fresnel PTFs in our numerical calculations. The Fresnel calculation is faster in general, whereas the Huygens kernel gives better quality images, especially at close range.

To achieve as high a lateral resolution as possible, one keeps the object-hologram distance as short as possible, but the discrete Fourier transform entails a certain minimum on this distance:

$$z_{\min} = \frac{a_x^2}{n_x\lambda}. \tag{11}$$

For an object of size a_x at a distance z from the hologram plane, the interference fringe spacing with a plane reference wave can be as small as $\lambda z/a_x$, which should be kept larger than the pixel size of the digital hologram. If the size of the hologram is also a_x and it has n_x pixels, then Eq. (11) follows. At too close a distance, the spatial frequency of the pixelated hologram is not high enough to reproduce a large angular size of the object without aliasing. For example, to image a 1×1-mm area of an object with 380×380 pixels
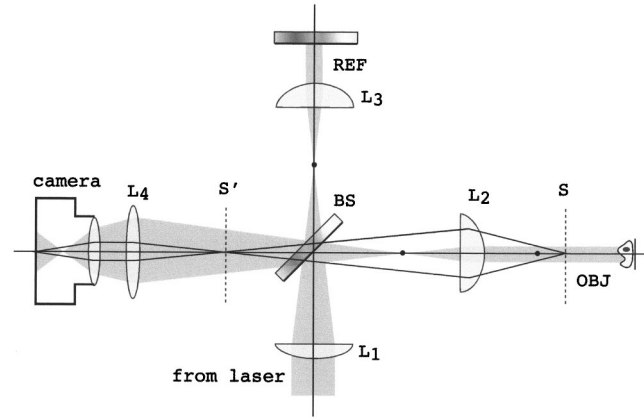
Fig. 2 Optical apparatus used in the digital interference holography experiments. The *L*s are various lenses; *BS* is a beamsplitter; and *M* is a mirror. The CCD camera captures the interference pattern at the plane *S*, as magnified at intermediate image plane *S'*.

using $\lambda=600$ nm, the minimum object distance is $z_{\min} = 4.4$ mm. Normally, we place the object just outside the minimum distance.

The procedure is repeated for N wavelengths $\lambda_m = \lambda_0 + m\Delta\lambda$ ($m = 0,1,2,...,N-1$), generating N 3-D arrays of complex numbers representing the electric fields that exist in the volume around the object under illumination of N different wavelengths. The N 3-D arrays are added together for superposition of these fields, resulting in a 3-D map of the object's structure. Since the phase of the laser field most likely fluctuates between wavelength changes, it is necessary to add a global phase factor to each of the N 3-D arrays. Specifically, out of each 3-D array of a calculated complex field, we sample a pencil of electric field values $E(x_p,y_p,z)$, where a 2-D position (x_p,y_p) is chosen to be a convenient point on the object. Numerical superposition of two of these pencils of fields for two different wavelengths shows the cosine-squared variation of two-wavelength interference. The phase-matching process then consists of making sure that the maxima occur at the same z distance by choosing an appropriate relative phase factor for each pair of wavelengths. Each of the 3-D arrays then gets multiplied globally by the corresponding phase factor. At this stage of development, this is done manually, but the procedure can be automated with a simple algorithm in the future. The resultant 3-D array is a representation of the surface—and possibly subsurface profile—in the case of reflection geometry of the object illumination. Or it can be a profile of the index and thickness variation, in the case of transmission geometry.

4 Experiments

The optical apparatus is a Michelson interferometer, as shown in Fig. 2. The laser source is a Coherent 699 ring dye laser, whose output is usually attenuated to about 50 mW. The system of lenses L_1 through L_4 is used to magnify the holographic interference pattern as captured by the CCD camera. The plane S is just outside the minimum distance $z_{\min}$ from the object. This plane is imaged to S' by the lens L_2, which in turn is imaged at infinity by the lens L_4 and finally recorded by the camera focused at infinity.
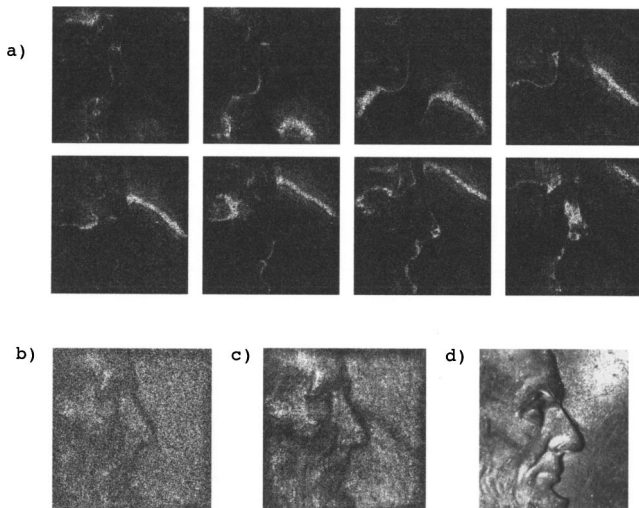
Fig. 3 Images of Lincoln's profile on a penny: (a) contour images; (b) single-wavelength hologram image; (c) flat view; and (d) photographic image with white light illumination. The area is 5×5 mm.

The lens L_1 provides plane-wave illumination of the object by focusing the input laser at the front focus of L_2. Collimating the reference beam with L_3 then results in a magnified image at S' of an interference pattern that would exist at S if the object wave is superposed with a plane wave there. Although not indicated in Fig. 2, the object and reference beams are tilted with respect to each other in an off-axis hologram arrangement to avoid the twin-image problem, and to improve zero-order suppression, both effects being implied by Eq. (4). When this is done, the two conjugate images (OR^* and O^*R) appear on the opposite sides of the bright zero-order spot ($|O|^2$ and $|R|^2$) in the reconstructed hologram. A number of LabView and MatLab programs are used for control of the experiment, numerical computations, and presentation of resulting images.

Some of the images from these preliminary experiments are shown in Figs. 3 and 4. Figure 3(a) is a series of contour images of the profile of Lincoln on a penny, generated from a set of 30 holograms taken with 1.06-nm increments of wavelengths starting at 575.0 nm. The image volume is
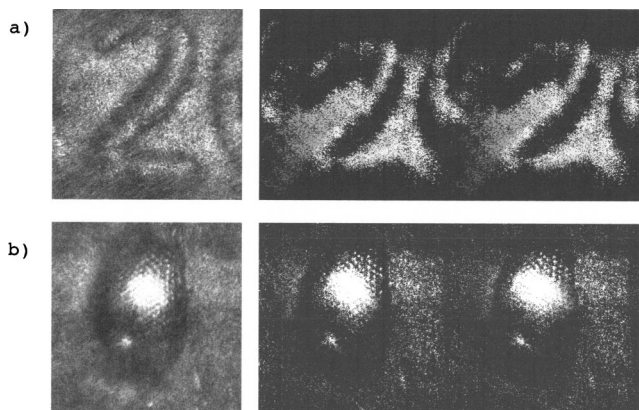
Fig. 4 (a) Flat and stereoscopic images of a numeral 2 in the 2000 mintage mark of a penny. The area is 1×1 mm. (b) Fht and stereoscopic images of a fire ant's compound eye. The area is 1×1 mm.

5×5 mm$\times 330$ μm and $380 \times 380 \times 30$ pixels, so that the pixel resolution is $13 \times 13 \times 11$ μm. Eight of the thirty z contours are shown in Fig. 3(a). Some of the contour lines are only one or two pixels thick, around the nose or lips for example, demonstrating excellent axial and lateral resolution and contrast. For the purpose of comparison, we also display a single wavelength hologram image in Fig. 3(b); a frontal view of all 30 contours summed together (flat view) in Fig. 3(c); and a regular photographic image under white light illumination in Fig. 3(d). Note that the flat view has a signal averaging effect and the speckle noise is greatly reduced compared to the single-wavelength hologram, and the image quality approaches that of conventional photograph (also see Fig. 4). Once the 3-D image data are acquired, they can be presented in a number of different manners, including contour and perspective views, as well as stereoscopic views. Figure 4(a) shows the flat and stereoscopic views of the numeral 2 on the 2000 mintage mark of a penny. The image volume is 1×1 mm$\times 330$ μm and $380 \times 380 \times 30$ pixels, so that the pixel resolution is $2.6 \times 2.6 \times 11$ μm. A standard technique for viewing stereo pair's is to start with your eyes very close to the page. As you pull away, you would see two pairs of images: try to merge these into three images and try to focus on the center image. At a certain comfortable distance, the 3-D perception will occur. Figure 4(b) shows the flat and stereoscopic views of the compound eye of a fire ant. Here the image volume is 1×1 mm$\times 540$ μm and $380 \times 380 \times 52$ pixels, so that the pixel resolution is $2.6 \times 2.6 \times 10$ μm. The size of the individual lenses in the compound eye is measured to be about 25 μm, which is very well resolved by these images. (Quicktime movies of some of these images are available at http://chuma.cas.usf.edu/~myungkim.)

5 Conclusions

The experimental results presented here demonstrate 3-D imaging of objects with micron scale resolution using digital interference holography. The technique is capable of generating cross sectional images of the objects with clear focus and good suppression of coherent speckle noise, using a fairly simple optical system and straightforward numerical methods. The achieved resolution is ~10 μm in the axial direction and ~3 μm in the lateral direction, which are limited only by the present optical system and computer capacity. There is some indication of imaging of internal or subsurface structures in the image of an ant eye. We are in the process of conclusively demonstrating true subsurface tomographic imaging by digital interference holography.

References

1. M. K. Kim, "Tomographic three-dimensional imaging of a biological specimen using wavelength-scanning digital interference holography," *Opt. Express* **7**, 305–310 (2000).
2. M. K. Kim, "Wavelength scanning digital interference holography for optical section imaging," *Opt. Lett.* **24**, 1693 (1999).
3. R. A. Robb, *Three-Dimensional Biomedical Imaging*, John Wiley and Sons, New York (1998).
4. C. J. R. Sheppard and D. M. Shotton, *Confocal Laser Scanning Microscopy*, Springer-Verlag, Berlin (1997).
5. D. Huang, E. A. Swanson, C. P. Lin, J. S. Schuman, W. G. Stinson, W. Chang, M. R. Hee, T. Flotte, K. Gregory, C. A. Puliafito, and J. G.

Fujimoto, "Optical coherence tomography," *Science* **254**, 1178–1181 (1991).

6. J. A. Izatt, M. D. Kulkarni, K. Kobayashi, M. V. Sivak, J. K. Barton, and A. J. Welch, "Optical coherence tomography for biodiagnostics," *Opt. Photonics News* **8**(5), 41–47 (1997).

7. J. G. Fujimoto, W. Drexler, U. Morgner, F. Kärtner, and E. Ippen, "Optical coherence tomography: High resolution imaging using echoes of light," *Opt. Photonics News* **11**(1), 24–31 (2000).

8. B. W. Schilling, T. C. Poon, G. Indebetouw, B. Storrie, K. Shinoda, T. Suzuki, and M. H. Wu, "Three-dimensional holographic fluorescence microscopy," *Opt. Lett.* **22**(19), 1506–1508 (1997).

9. P. Hariharan, *Optical Holography: Principles, Techniques, and Applications*, Cambridge Univ. Press, Boston, MA (1996).

10. S. De Nicola, P. Ferraro, A. Finizio, and G. Perattini, "Correct-image reconstruction in the presence of severe anamorphism by means of digital holography," *Opt. Lett.* **26**, 974–976 (2001).

11. T. Zhang and I. Yamaguchi, "Three-dimensional microscopy with phase-shifting digital holography," *Opt. Lett.* **23**, 1221 (1998).

12. U. Schnars, M. Thomas, and W. P. Jueptner, "Digital recording and numerical reconstruction of holograms: Reduction of the spatial frequency spectrum," *Opt. Eng.* **35**(4), 977–982 (1996).

13. N. H. Abramson and K. G. Spears, "Single pulse light-in-flight recording by holography," *Appl. Opt.* **28**, 1834–1841 (1989).

14. B. P. Hildebrand and K. A. Haines, "Multiple-wavelength and multiple-source holography applied to contour generation," *J. Opt. Soc. Am.* **57**, 155 (1967).

15. N. George and W. Li, "Holographic contouring by using tunable lasers," *Opt. Lett.* **19**, 1879–1881 (1994).

16. Z. He and K. Hotate, "Synthesized optical coherence tomography for imaging of scattering objects by use of a stepwise frequency-modulated tunable laser diode," *Opt. Lett.* **24**, 1502–1504 (1999).

17. J. C. Marron and T. J. Schulz, "Three-dimensional, fine-resolution imaging using laser frequency diversity," *Opt. Lett.* **17**, 285–287 (1992).

18. Yu T. Mazurenko, "Holography of wave-packets," *Appl. Phys. Lett.* **B50**, 101–114 (1990).

19. J. W. Goodman, *Introduction to Fourier Optics, 2nd ed.*, McGraw-Hill, New York (1996).

Aaron Dakoff graduated from the University of South Florida with a BS in physics in 2000 and a MS in physics in 2002. His graduate thesis was entitled "Tomography of diffuse objects through distorting media using wavelength scanning digital interference holography." While his main research focus is 3-D microscopic imaging, other past projects have included holographic phase mapping and topographic imaging.

James Gass graduated from University of South Florida with a BS in physics in 2000 and a MS in physics in 2002. His thesis title was "Elimination of 2π ambiguity through two wavelength interference using digital holography." His main research interest is microscopic imaging. Past projects include wavelength scanning digital interference holography and holographic phase mapping.
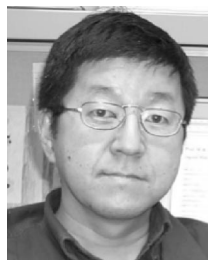
Myung K. Kim received the BS degree in physics and mathematics from the University of California, Los Angeles, in 1979, and the PhD degree in physics from the University of California, Berkeley, in 1986. His postdoctoral training was at SRI International, Menlo Park, California. He was an assistant professor at Wayne State University in Detroit, Michigan, during 1988 to 1995, then he moved to the University of South Florida, Tampa, as an associate professor. His research interests have been time-domain laser spectroscopy, photon echo of gases and solids, holographic optical storage of spatiotemporal dimensions, and holographic image processing. Current emphasis of his research program is in the development of novel techniques in digital holography, phase imaging, scanning probe microscopy, and applications in biomedical imaging.